Local magnetism in palladium bionanomaterials probed by muon spectroscopy

Neil J. Creamer, Iryna P. Mikheenko, Clive Johnson, Stephen P. Cottrell, Lynne E. Macaskie

Section: Biofuels and Environmental Biotechnology

Local magnetism in palladium bionanomaterials probed by muon spectroscopy

Neil J. Creamer [a], Iryna P. Mikheenko [a], Clive Johnson [b], Stephen P. Cottrell [b] and Lynne E. Macaskie [a*]

[a] Unit of Functional Bionanomaterials, School of Biosciences, University of Birmingham, Edgbaston, Birmingham B15 2TT, UK

[b] ISIS, Science and Technology Facilities Council, Rutherford Appleton Laboratory, Didcot OX11 0QX, UK

Key words: Desulfovibrio desulfuricans, *electronic magnetism, muon spin rotation spectroscopy, nanoparticles, palladium bionanoparticles*

***Author for correspondence: L.E.Macaskie@bham.ac.uk**

Abstract

Palladium bionanomaterial was manufactured using the sulfate-reducing bacterium, *Desulfovibrio desulfuricansm*, to reduce soluble Pd(II) ions to cell-bound Pd(0) in the presence of hydrogen. The biomaterial was examined using a Superconducting Quantum Interference Device (SQUID) to measure bulk magnetisation and by Muon Spin Rotation Spectroscopy (μSR) which is uniquely able to probe the local magnetic environment inside the sample. Results showed behaviour attributable to interaction of muons both with palladium electrons and the nuclei of hydrogen trapped in the particles during manufacture. Electronic magnetism, also suggested by SQUID, is not characteristic of bulk palladium and is consistent with the presence of nanoparticles previously seen in electron micrographs. We show

the first use of μSR as a tool to probe the internal magnetic environment of a biologically-derived nanocatalyst material.

Introduction

There is substantial current interest in nanoparticles as they often exhibit properties at odds with those of the bulk material (Hori et al. 1999, Eberhardt 2002). Palladium nanoparticles have been extensively studied both experimentally and theoretically mainly due to the excellent performance of the metal as a catalyst in hydrogenation and hydrogenolysis (Schuth and Reinhard 1998; Nishimura 2001). A recent development is the production of Pd nanoparticles supported on bacterial cells which show excellent potential as catalysts (Creamer et al. 2007) in applications such as remediation of Cr(VI) (Mabbett et al. 2006), chlorinated aromatic compounds (Baxter-Plant et al. 2003; Redwood et al. 2008), pesticides (Mertens et al. 2007) and chlorinated organophosphates (Deplanche et al. 2009), as well as major potential applications in 'green chemistry' (Bennett et al. 2010; Wood et al. 2010) and in clean energy (Yong et al. 2007; 2010; Orozco et al. 2010). The nanoparticulate nature of catalytically-active 'Bio-Pd' was shown by surface area measurements (Bennett et al. 2010) while, using a magnetic method, Mikheenko et al (2001) showed the presence of nanoparticles of size ~ 5 nm.

The free Pd atom is non-magnetic and, in bulk, no spontaneous ferromagnetic order has been observed (Staunton et al. 2000; Vega et al. 2003). However, studies of palladium nanoparticles formed by gas evaporation demonstrated ferromagnetism in a population of particles with mean diameter 5.9 nm (Taniyama et al. 1997) which has been attributed to non-typical metal–metal bonding due to the constraints of the particle size (Vitos et al. 2000).

The early finding that Bio-Pd particles are magnetically active (Mikheenko et al. 2001) together with the observation that the magnetic moment, nanoparticle size and hence catalytic activity are related (Macaskie et al. 2005) is important because these can be controlled by the choice of preparation conditions. In general mid-logarithmic and early stationary-phase cells give the smallest nanoparticles (Mikheenko 2004). This degree of control makes the material very appropriate for this examination. In order to visualise the magnetic components we used two preparations of the same mass loading of Pd(0),

made using two cultures of the same strain. These provide a common background biomatrix on which to evaluate the potential of μSR as a tool for characterisation of metallic bionanoparticles.

The muon is an unstable lepton with a mean lifetime of ~2.20 μs. It has a magnetic moment approx. three times that of the proton and, in studies of condensed matter, is essentially a sensitive microscopic magnetometer (Dalmas de Reotier and Yaouanc 1997). For the systems studied here, positive muons typically thermalise at an interstitial location and thus probe the local magnetic fields in the regions between the atoms. The ISIS synchrotron produces a beam of positive muons with a unique momentum (29.8 MeV/*c*) which is 100% spin-polarised (ISIS web page). Unlike other particle probes, muons stop within the sample before decaying into a positron and two neutrinos. Crucially, the positron is emitted preferentially in the direction of the muon spin enabling the time evolution of the muon polarisation (or decay asymmetry) to be followed by detecting the time dependence of the positron distribution. Thus it is possible to measure the time dependent depolarisation of the muon signal and characterise the distribution and dynamics of internal fields in the sample.

The μSR experiment is sensitive to both nuclear and electronic magnetism (Dalmas de Reotier and Yaouanc 1997). Where implanted muons interact with the static, dipolar fields associated with nuclei, the asymmetry decay function reflects the distribution of fields and is typically Gaussian in form. For an ordered electronic system a coherent precession of the muon polarisation may be seen provided muons thermalise into a limited number of unique sites. At ISIS the instrument pass-band (~6 MHz) will also limit the frequencies that can be measured, and instead an ordered state may be revealed by the loss of 2/3 of the initial asymmetry. Fluctuating electronic moments (due to unpaired spins) may also be measured, when the decay is typically described by a Lorentzian function.

In insulating materials, the implanted muon may bind an electron to form muonium, an exotic light hydrogen isotope with the positive muon as the nucleus (Cox 1987). This species may, in turn, react with organic systems to form radical states: in both cases the muon-electron hyperfine coupling complicates the signal measured and determining the fractions of the various muonic states present in the system is an important aspect of the experiment.

Prior to this study, Kemali et al. (1997) had applied μSR to the study of heavily dislocated hydrogen-containing bulk Pd. Kaiser et al. (2003) investigated monodisperse, ligand-capped Pd nanoparticles of diameter 1.1 nm, smaller than most of the particles studied here (see Mikheenko et al. 2001) but close to the 1.2 to 6 nm critical size range within which Pd is expected to demonstrate super-paramagnetic/ferromagnetic behaviour (Taniyama et al. 2007; Staunton et al. 2000). In that study, the Pd particles were capped by a ligand shell of diameter ~2.1 nm, while here they are supported in a biomatrix which extends to the micron scale. The current study is the first application of μSR as a probe for catalytic bionanoparticles.

Materials and Methods

Manufacture of palladium on bacterial cells (Bio-Pd)

Palladium bionanomaterial was manufactured by exposing resting cells of *Desulfovibrio desulfuricans* NCIMB 8307 (cultures harvested at different stages of growth to give samples of different magnetic activity, e.g. see Macaskie et al. 2005) to an anaerobic solution (pH 2.3) of Na_2PdCl_4 (Aldrich, 99.995 %) such that the total palladium available was 25% of the calculated dry cell weight (Lloyd et al. 1998). Following biosorption of soluble Pd(II) ions the suspension was sparged with H_2 for 30 minutes resulting in the formation of palladium particles in the periplasmic space and at the cell surface (e.g. Baxter-Plant et al. 2003; Macaskie 2005; Mikheenko et al. 2008). Cells were washed in distilled water three times then once in acetone, air dried and ground to a fine powder. For the purposes of this study, two separate batches were prepared: ‘Sample 1’ was from an early stationary phase culture while ‘Sample 2’ was harvested in the mid-growth phase.

Magnetic measurements using a superconducting quantum interference device (SQUID)

The magnetic moments (emu/g) of the two biological palladium powders and, for reference, high purity Pd powder (Johnson Matthey, 99.998 %) were measured in a superconducting quantum interference device (SQUID: Quantum Design, USA) against the applied magnetic field (H, Oersted). The magnetic

field was varied between zero and 10,000 Oe. All measurements are expressed per g of palladium and accuracy is limited by mass determination to ±10%. SQUID data were collected as described previously (Mikheenko 2001) by measuring the dependence of the magnetic moment on the applied field.

Magnetic measurements using Muon Spin Rotation Spectroscopy (μSR)

The μSR experiments were carried out using the EMU spectrometer at the ISIS pulsed muon source (ISIS web page). This instrument is configured with detectors forward (upstream) and backward (downstream) of the sample, and is ideal for the zero and longitudinal field (<4,500 G) measurements carried out in this work. For this instrument, the muon spin polarisation is co-linear with the beam momentum. The samples were mounted in a 24 mm diam.-recessed aluminium sample holder with a silver mask placed around the sample to ensure a predictable response from muons stopping outside the sample area. Temperature control was achieved using a closed-cycle refrigerator with the sample attached by a suitable cold-finger.

Data is initially reduced using Equation 1 to form the time dependent decay asymmetry for the counts recorded in the forward (N_F) and backward (N_B) detectors for the 32 μs measured following muon implantation:

$$a(t) = [N_F(t) - \alpha N_B(t)] / [N_F(t) + \alpha N_B(t)] \quad (1),$$

where α is a parameter describing the relative efficiencies of the forward and backward detector arrays that is calibrated for each sample mounted on the spectrometer by applying a small external field transverse to the muon polarisation.

The time dependent behaviour of the decay asymmetry takes the form:

$$a(t) = a_0 G_z(t) \quad (2),$$

where $G_z(t)$ is a function describing the time evolution of the muon spin polarisation due to spin interactions and a_0, the full asymmetry for the EMU spectrometer (~23%). Analysis is completed by least squares fitting of the appropriate form of $G_z(t)$ to the reduced data.

Results and discussion

The magnetisation of samples 1 and 2 was determined by SQUID measurements to provide a reference for the μSR study. The bulk Pd control gave a linear response of magnetic moment against the applied field, whereas the two samples showed a non-linearity (Fig 1A,B). From our results, we calculate that the average moment per nanoparticle in Sample 1, 1 to 3×10^2 μ_B, is consistent with electronic magnetism in Pd grains of size ~ 4–6 nm assuming either that all atoms in the particle contribute equally to the overall magnetism each having a moment of 0.11 μ_B (Vitos et al. 2000) or that only the surface atoms contribute and each atom has a moment of 0.23 μ_B (Taniyama et al. 1997). These estimates also lie within the size range of 1.2 to 6 nm for which ferromagnetism has previously been observed (Taniyama et al. 2007; Staunton et al. 2000).

As shown in Figs. 1A and 1B, Sample 2 had a significantly larger non-linear component than Sample 1, suggesting a larger proportion of small particles within the range of 1.2 to 6 nm. Skibar et al. 2005) showed that for a given microbial support (*D. desulfuricans*) the non-linear component can range from being practically zero to almost 100 % according to how the samples are prepared (e.g. by using the Pd amine salt instead of the chloride salt and a neutral instead of acidic pH during Pd-challenge) as well as the growth phase from which the culture was harvested. Examples were shown previously (Macaskie et al. 2005). For the present study, and from the SQUID characterisation shown in Figs. 1A and 1B, Samples 1 (‘magnetic’) and 2 (‘non-magnetic’) were chosen as providing suitable references with which to evaluate the scope for using μSR to provide specific information about local magnetic effects within the samples.

The system under study comprises hydrogen-containing palladium nanoparticles (25% by mass) supported in dried biomatrix (75% by mass); implanted muons may stop in either the nanoparticles or the biomatrix approximately according to their mass fractions although additional stops in the metal particles cannot be ruled out (Ma et al. 2007). To allow comparison, care was taken to ensure Samples 1 and 2 had the same mass ratio of nanoparticle to biomatrix. For muons thermalising in the biomass muonium or radical states may be formed, while the biological material also contains trace Fe associated with redox enzymes that might also give rise to local electronic fields. Muons stopping in (or close to) the Pd particles may interact with both the electronic or nuclear fields associated with the

metal atoms or the trapped hydrogen. The latter has a significant nuclear magnetic moment as evidenced by its usefulness as a target for NMR Spectroscopy (Harris 1996). Measurements of the non-magnetic Sample 1 can provide a good indication as to the various muonic states forming in this system and, accordingly, this was the focus of the initial study.

Zero applied magnetic field measurements were carried out for Sample 1 between 10 K and 300 K. Throughout this temperature range the form of the muon spin relaxation observed could be modelled by a two-component function comprising a Gaussian decay and a non-relaxing background, as described by equation (3):

$$a(t) = a_0 \exp [- (\sigma t)^2] + a_b \qquad (3).$$

In the present analysis, the background term, a_b, subsumed both a large non-relaxed fraction originating from the sample and a much smaller signal arising from muons stopping in the surrounding silver mask. The relaxation rate, σ, reflects the distribution of local fields at the muon site.

The total asymmetry of the zero field signal is roughly constant at ~ 22 % over the full temperature range, with corresponding 100 G transverse field data confirming this to be diamagnetic in origin. This result suggests muonium formation in the biomatrix is minimal (< 1 % asymmetry) – a fortunate outcome that greatly simplifies analysis of this system. The asymmetry of the Gaussian component remains constant, however, over a broad temperature range at ~6 %, suggesting that ~25% of the muons are consistently implanted into a similar environment. The temperature dependence of the relaxation rate, σ, is shown in Figure 2. Intriguingly, at low temperatures, the rate is similar to the value of 0.24 μs^{-1} reported for muons stopping in the hydrogen-saturated dislocated Pd metal (Kemali et al.1997). Furthermore, the peak in the rate measured at ~75 K is consistent with the onset of mobility and subsequent trapping, although the precise nature of the trapping sites (whether in the bulk or at the surface) remains to be determined.

Considering these results, it seems unlikely that the Gaussian component could originate from the biomatrix, with the signal probably due to muons stopping in the Pd nanoparticles. While the moment on the Pd nucleus is small, and in itself will make only a small contribution to the measured depolarisation, hydrogen is known to be incorporated into the nanoparticle structure during manufacture

and, assuming suitable traps, the interaction of its large nuclear moment with the implanted muon can explain the form of the measured signal. As the temperature is increased above 75 K there is a gradual reduction in the measured linewidth that continues to the highest temperature measured (300 K), a result suggesting the onset of mobility of the muon relative to the hydrogen in the nanoparticle structure. The weak relaxation of muons stopping in the biomatrix is surprising as the organic material is also likely to contain hydrogen; we assume that the preferred muon site and/or dynamics contrive to limit the local field on the muon.

Similar μSR measurements were carried out on Sample 2 which was shown from SQUID measurements to have an electronic magnetic signature. Immediately apparent is the substantial missing fraction present in both the zero field (evident in the first points plotted in Fig 4B) and the 100 G transverse field data (see Fig 3A). The measured transverse asymmetry of ~14.5 % at room temperature suggests a missing fraction of ~7 % in asymmetry. Since the mass fraction and composition of the biomatrix is maintained compared to the non-magnetic Sample 1, a near identical stopping distribution is expected with almost all muons thermalising into a diamagnetic state. Although Fe impurities are present in the biomatrix, there was no evidence from the measurements on Sample 1 that these are magnetically active and contributing to the signal. Futhermore, other studies using element-specific X-ray magnetic circular dichroism confirmed that the magnetic signal of the specimen was specifically attributable to Pd (N.J. Creamer, I. Mikheenko and L.E. Macaskie, unpublished work). The asymmetry loss is similar to the signal amplitude measured from the Pd nanoparticles in Sample 1, and it therefore seems likely that muons stopping in and adjacent to the nanoparticles are experiencing a substantial magnetic field that depolarises the muon signal between implantation and the start of measurement.

To investigate the internal field strength of the magnetic nanoparticles and the associated field on the implanted muon, a longitudinal field decoupling measurement was carried out. Here, large external fields are applied and the initial muon asymmetry is recovered as these dominate the internal fields of the sample. The result of such a measurement is shown in Figure 3A. Even applying 4000 G, the strongest field available on the instrument, the field was insufficient to fully recover the full initial

asymmetry; however, its dependence on the applied field is clear and the mid-point of the decoupling curve enables us to estimate the internal field at the muon site to be ~1000 G. While these measurements suggest the nanoparticles as the source of the bulk fields measured by the SQUID, a more detailed understanding of muon trapping in this system is required to properly correlate the data. The overall shape of the curve suggests that muons are sampling a broad distribution of internal fields; however, this is a reasonable result given the highly inhomogeneous nature of the sample and the absence of a unique muon site. As expected, the longitudinal relaxation, obtained from fitting an exponential decay, is quenched as the applied field is increased (Figure 3B). For comparison, a similar measurement is shown for Sample 1 where there is clearly no dependence of the signal asymmetry on the applied field.

Since the fraction of muons implanted into the Pd nanoparticles is rapidly depolarised by strong internal fields, the zero field asymmetry measured for Sample 2 must originate from muons stopping in the biomatrix and sample holder. In contrast to the non-magnetic sample, where the signal from the biomatrix was non-relaxed, a significant decay was measured over the full temperature range for the magnetic system, with representative spectra shown in Figure 4A. Relaxation of the muon signal is not surprising since the magnetic nanoparticles are effectively forming a dilute spin system within the biomatrix. SQUID measurements demonstrate the nanoparticles to have a substantial magnetic moment ($1 - 3 \times 10^2$ μ_B, see above), and therefore there will be a field profile associated with each nanoparticle falling as r^{-3} to leave a region of field inhomogeneity between the nanoparticles. The temperature dependence of the relaxation signal is probably the result of dynamics, a conclusion supported by parameterising the data using the stretched exponential form defined in equation 4:

$$a(t) = a_0 \exp [-(\lambda t)^{\beta}] \qquad (4).$$

From fitting the data we find that the exponent, β (Fig 4B, open circles), changes from ~1.6 (tending towards a Gaussian form) at low temperature to ~1 (a simple exponential) at 300 K while the relaxation rate, λ (Fig 4B, closed circles), shows a slow reduction with increasing temperature. Attempting to apply models, such as the root exponential form, used in the analysis of other dilute magnetic systems (e.g. Kaiser et al. 2003; Bewley and Cywinski 1998; Lord 2005) has not been successful, possibly

because of the potential for multiple muon sites and complex dynamics within the present material. Further work is clearly required to establish the nature of the dynamics observed in this material.

Conclusions

SQUID measurements have demonstrated bulk magnetism in palladium nanoparticles supported in a biomatrix. This paper reports the first application of the local magnetic field probe, μSR, to identify the source of electronic magnetism within this system. Comparative measurements between two samples showing strong and weak bulk electronic magnetism have enabled us to identify a fraction of muons stopping within the palladium nanoparticles. The behaviour of this fraction is indicative of local coupling between the implanted muon and strong magnetic fields associated with the individual palladium nanoparticles present in a magnetic sample, a result consistent with measurements using element-specific X-ray Circular Magnetic Dichroism (XMCD) to be published at a later date.

Analysis of the muon signal has shown that almost 75% of the implanted muons thermalise in the biomatrix and are sensitive to the dynamics within the system. Measurements on Sample 2 suggest that electronic spin fluctuations persist throughout the temperature range studied. We tentatively conclude that these are associated with the electronic magnetism observed in the individual palladium nanoparticles. Further experimental work using μSR is needed to properly characterise the nature and source of these dynamics.

Acknowledgements

We acknowledge with thanks the financial support of the EU (Contract No. G5RD-CT-2002-0075), the BBSRC (Grant Nos BB/C516195/2 and BB/E003788/1) and the EPSRC (Grant Nos EP/D05768X/1 and EP/E034888/1).

References

Baxter-Plant VS, Mikheenko IP, Macaskie LE (2003) Sulphate-reducing bacteria, palladium and the reductive dehalogenation of chlorinated aromatic compounds. Biodegradation 14:83-90

Bennett JA, Creamer NJ, Deplanche K, Macaskie LE, Shannon IJ, Wood JA (2010) Pd supported on bacteria and biomass as a novel heterogeneous catalyst: a comparison of Pd_2AlO_3 and Bio-Pd in the hydrogenation of 2-pentyne. Chem Eng Sci 65: 282-290

Bewley RI, Cywinski R (1998) Muon spin relaxation in a superparamagnet: Field dynamics in $Cu_{98}Co_2$. Phys Rev B 58: 11544-11551

Cox SFJ (1987) Implanted muon studies in condensed matter science. J. Phys. C: Solid State Phys. 20 3187-3318

Creamer NJ, Mikheenko IP, Deplanche K, Yong P, Wood J, Pollmann K, Selenska-Pobell S, Macaskie LE (2007) A novel hydrogenation and hydrogenolysis catalyst using palladized biomass of Gram negative and Gram positive bacteria. Biohydrometallurgy 20-21: 603-606

Dalmas de Reotier P, Yaouanc A (1997) Muon spin rotation and relaxation in magnetic materials. J Phys-Condens Matter 9: 9113-9166

Deplanche K, Snape TJ, Hazrati S, Harrad S, Macaskie LE (2009) Versatility of a new bioinorganic catalyst: palladized cells of *Desulfovibrio desulfuricans* and application to dehalogenation of flame retardant materials. Environ Technol 30:681-692

Eberhardt W (2002) Clusters as new materials. Surf Sci 500: 242-270

Harris RK (1996) Encyclopedia of Nuclear Magnetic Resonance. Granty DM and Harris RK (eds.) John Wiley & Sons, Chichester, UK.

Hori H, Teranishi T, Nakae Y, Seino Y, Miyake M, Yamada S (1999) Anomalous magnetic polarization effect of Pd and Au nano-particles. Phys Lett A 263: 406-410

ISIS from http://www.isis.rl.ac.uk/archive/Muons/muonsIntro/index.htm.

Kaiser CT, Gubbens PCM, Mulder FM, Dalmas de Reotier P, Yaouanc A, Paulus P, de Jongh LJ, Schmid G, King PJC, Amato A (2003) μSR investigation of a cluster of monodisperse Pd nanoparticles. Physica B 326: 484–488

Kemali M, Ross DK, Cottrel SP (1997) Trapped muon in heavily dislocated palladium. J Alloy Compd 253: 420-422

Lloyd, JR, Yong P, Macaskie LE (1998) Enzymatic recovery of elemental palladium by using sulfate-reducing bacteria. Appl Environ Microbiol 64: 4607-4609

Lord JS (2005) Muon methods for studying nanomagnetism J. Phys.:Conf. Ser. 17 81-86

Ma L, Wang Y, Xue J, Chen Q, Zhang W, Zhang Y (2007) Energy loss and straggling of MeV ions through biological bamples. J Appl Phys: 102 084702

Mabbett AN, Sanyahumbi D, Yong P, Macaskie LE (2006) Biorecovered precious metals from industrial wastes: single step conversion of mixed metal liquid waste to bioinorganic catalyst ["MMBio-Pd(0)"] with environmental application. Environ Sci Technol 40:1015-1021

Macaskie LE, Baxter-Plant VS, Creamer NJ, Humphries AC, Mikheenko IP, Mikheenko PM, Penfold DW, Yong P (2005) Applications of bacterial hydrogenases in waste decontamination, manufacture of novel bionanocatalysts and in sustainable energy. Biochem Soc Trans 33: 76–79

Mertens B, Blothe C, Windey K, DeWindt W, Verstraete W (2007) Biocatalytic dechlorination of lindane by nanoscale particles of Pd(0) deposited on *Shewanella oneidensis*. Chemosphere 66: 99-105

Mikheenko IP (2004) Nanoscale palladium recovery. PhD Thesis University of Birmingham UK

Mikheenko IP, Mikheenko PM, Darlington CNW, Muirhead CM, Macaskie LE (2001) Magnetic testing of Pd-loaded bacteria. In Biohydrometallurgy: Fundamentals, Technology and Sustainable Development Ciminelli VST and Garcia O Jr. (eds) Elsevier, Amsterdam, ISBN 0444 50623 3 pp 525-532

Mikheenko IP, Rousset M, Dementin S, Macaskie LE (2008) Bioaccumulation of palladium by *Desulfovibrio fructosovorans* and hydrogenase deficient mutants, Appl Environ Microbiol 19: 6144-6146

Nishimura S (2001) Handbook of Heterogeneous Catalytic Hydrogenation for Organic Synthesis. New York, Chichester, Wiley.

Orozco RL, Redwood MD, Yong P, Caldelari I, Sargent F, Macaskie LE (2010) Towards an integrated system for bio-energy: Hydrogen production by *Escherichia coli* and use of palladium-coated waste cells for electricity generation in a fuel cell. Biotechnol Letts 32: 1837-1845

Redwood MD, Deplanche K, Baxter-Plant VS, Macaskie LE (2008) Biomass-supported catalysts on *Desulfovibrio desulfuricans* and *Rhodobacter sphaeroides*. Biotechnol Bioeng 99: 1045-1054

Schuth C, Reinhard M (1998) Hydrodechlorination and hydrogenation of aromatic compounds over palladium on alumina in hydrogen-saturated water. Appl Catal B-Environ 18: 215-221

Skibar W, Macaskie LE, Rousset M, Fratzl P, Pompe W, Selenska-Pobell S (2005) Novel precious metal-based bionanocatralsyst from scrap. Final Report EU contract G5RD-CT-2002-00750

Staunton JB, Poulter J, Ginatempo B, Bruno E, Johnson DD (2000) Spin fluctuations in nearly magnetic metals from *ab initio* dynamical spin susceptibility calculations: Application to Pd and $Cr_{95}V_5$. Phys Rev B 62: 1075-1082

Taniyama T, Ohta E, Sato T (1997) Ferromagnetism of Pd fine particles. Physica B 237: 286-288

Vega A, Parlebas JC, Demangeat C (2003) Electronic structure calculations of low-dimensional transition metals. Handbook of magnetic materials. KHJ Buschow. Amsterdam, Elsevier Science: 199-288

Vitos L, Johansson B, Kollar J (2000) Size-dependent paramagnetic-ferromagnetic phase transition in palladium clusters. Phys Rev B 62: 11957-11960

Wood J, Bodenes L, Bennett JA, Deplanche K, Macaskie LE (2010) Hydrogenation of 2-butyne-1,4-diol using novel bio-palladium catalysts. Indust Chem Eng Res 49: 980-988

Yong P, Paterson-Beedle M, Mikheenko IP, Macaskie LE (2007) From bio-mineralisation to fuel cells: biomanufacture of Pt and Pd nanocrystals for fuel cell electrode catalyst. Biotechnol Letts 29: 539-544

Yong P, Mikheenko IP, Deplanche K, Redwood MD, Macaskie LE (2010) Biorefining of Precious Metals from Wastes-An Answer to Manufacturing of Cheap Nanocatalysts for Fuel cells and Power Generation via an Integrated Biorefinery? Biotechnol Letts 32:1821-1828

Legends to Figures

Fig 1: Magnetic field dependence of the magnetic moment component for Sample 1 (A) and Sample 2 (B). ●: Total magnetisation ○: Non-linear. Note the magnitude difference of the *y*-axis in Fig. 1B compared to Fig 1A.

Fig 2 Temperature dependence of the zero-field relaxation rate measured in Sample 1 for the Gaussian component attributed to nuclear magnetism.

Fig 3. A: Longitudinal field dependence of asymmetry measured for Samples 1 and 2 at 300 K: ○: Sample 1 (low non-linear component as shown in Fig 1A). ● Sample 2 (high non-linear component as shown in Fig 1B). **B:** Longitudinal field dependence of relaxation rate measured for Sample 2 obtained from fitting the data with a simple exponential.

Fig 4. A: Representative zero field measurements for Sample 2 shown as a function of temperature. □ 15 K; ● 105 K; ○ 195 K; ■ 300 K. B: Stretched exponential analysis of data measured for Sample 2 showing both relaxation rate, λ ●, and exponent, β ○, obtained from fitting.

Figure 1

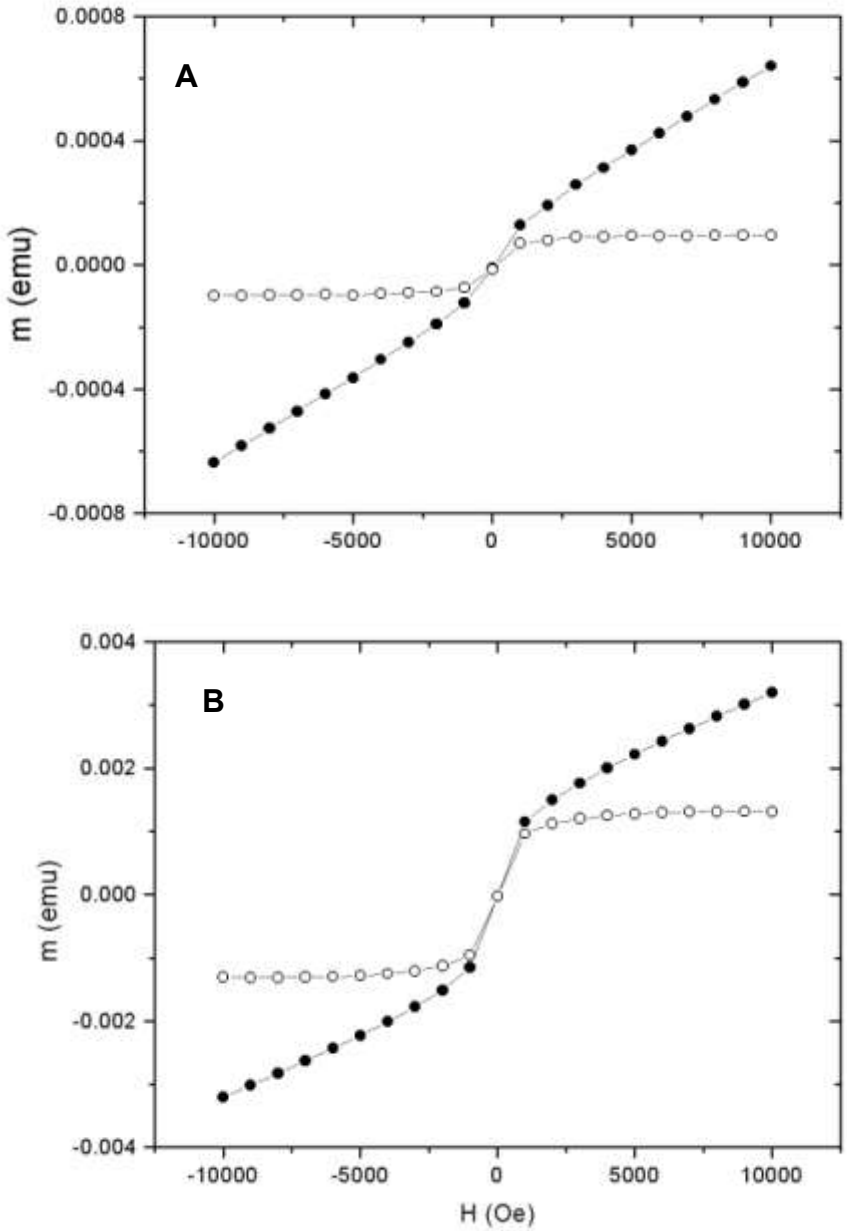
A
B
m (emu)
H (Oe)
0.0008
0.0004
0.0000
-0.0004
-0.0008
0.004
0.002
0.000
-0.002
-0.004
-10000
-5000
0
5000
10000

Figure 2

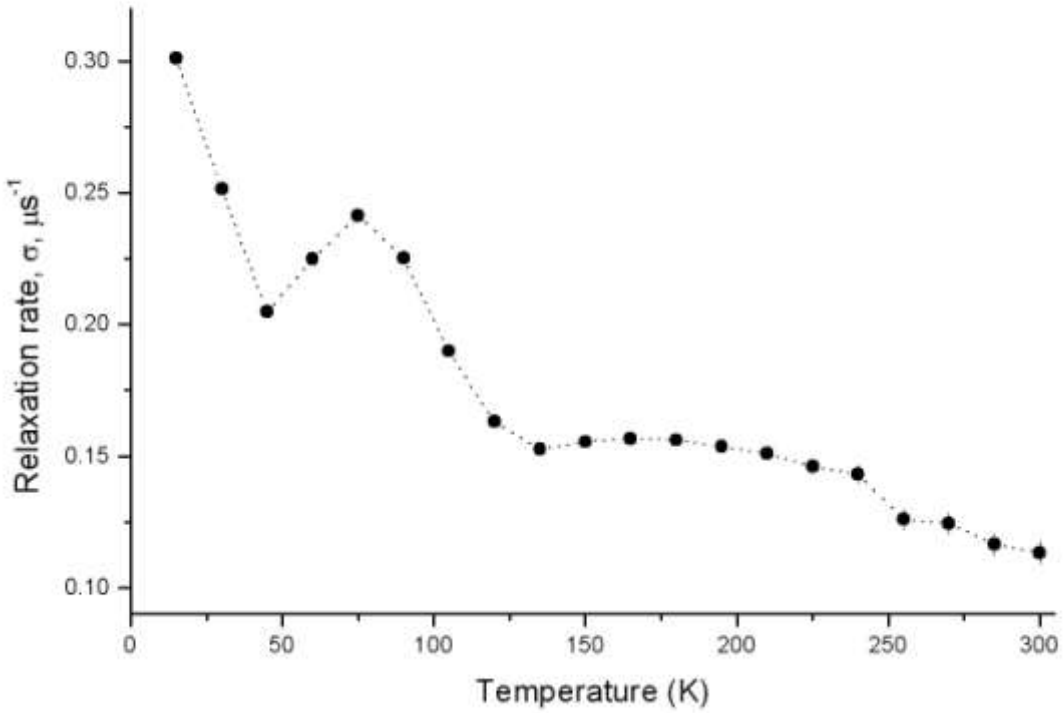
Relaxation rate, σ, μs-1
0.30
0.25
0.20
0.15
0.10
0
50
100
150
200
250
300
Temperature (K)

Figure 3

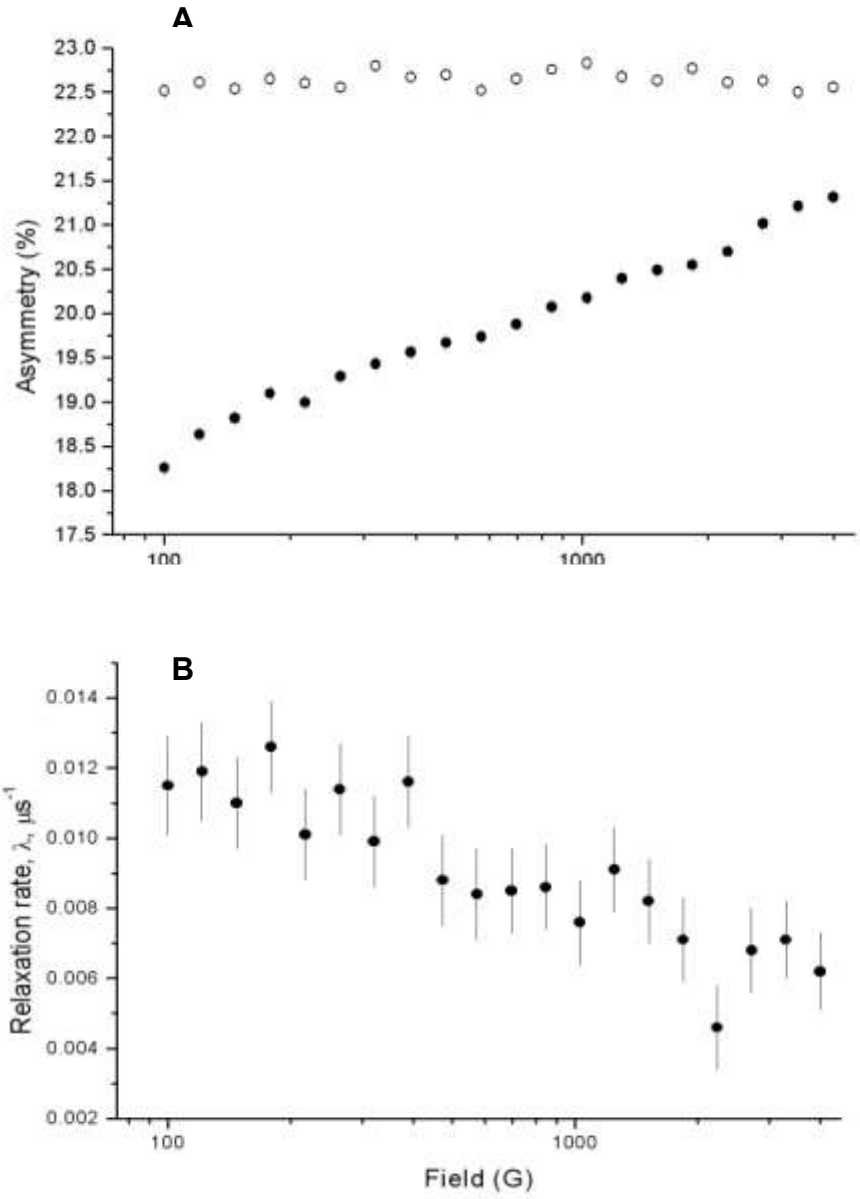
A
Asymmetry (%)
23.0
22.5
22.0
21.5
21.0
20.5
20.0
19.5
19.0
18.5
18.0
17.5
100
1000
B
Relaxation rate, λ, μs⁻¹
0.014
0.012
0.010
0.008
0.006
0.004
0.002
100
1000
Field (G)

Figure 4

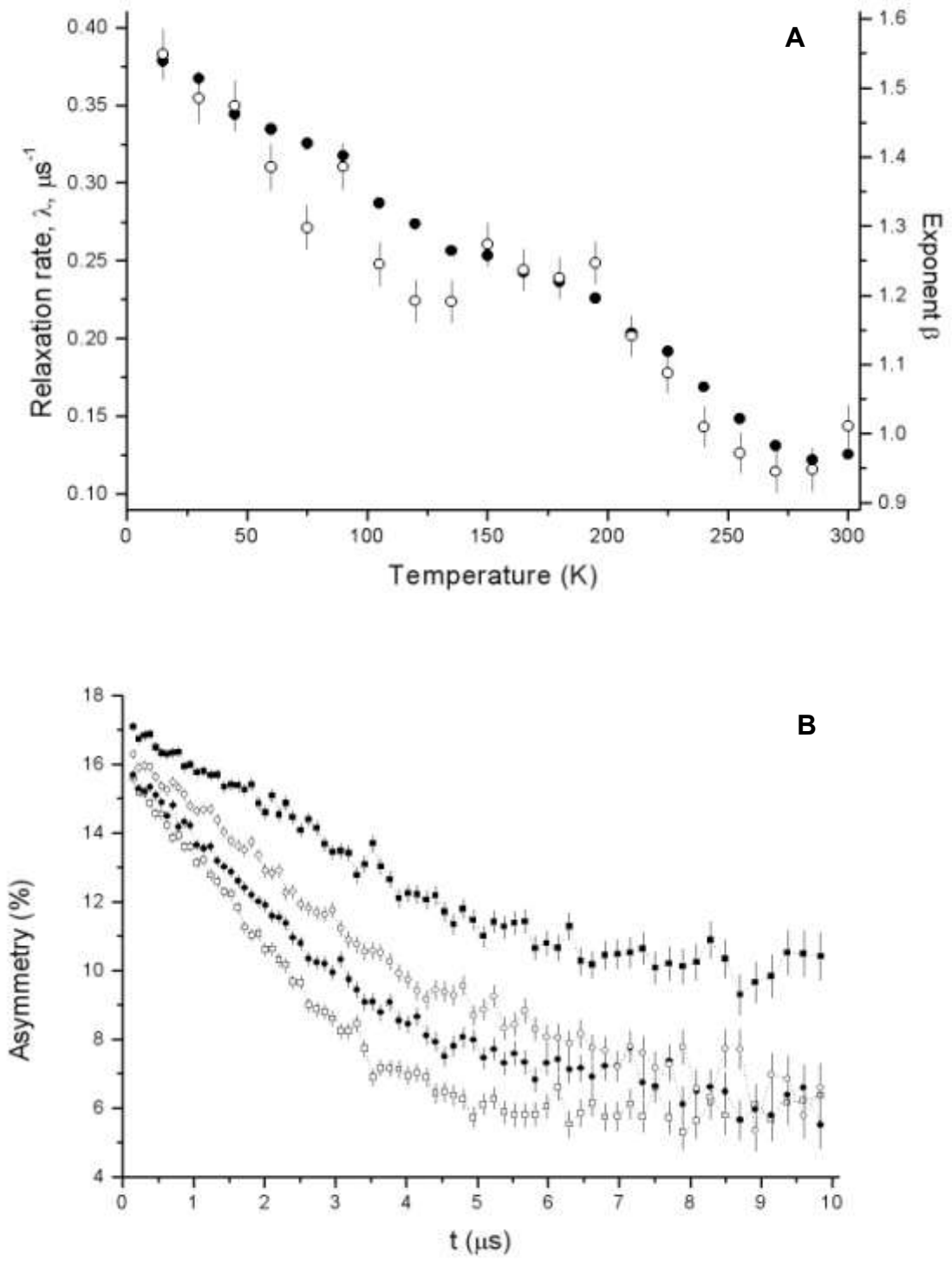
A
Relaxation rate, λ, μs⁻¹
Exponent β
Temperature (K)
0.40
0.35
0.30
0.25
0.20
0.15
0.10
1.6
1.5
1.4
1.3
1.2
1.1
1.0
0.9
0
50
100
150
200
250
300
B
Asymmetry (%)
t (μs)
18
16
14
12
10
8
6
4
0
1
2
3
4
5
6
7
8
9
10